Submitted to the International Europhysics Conference on High Energy Physics,
HEP97, Jerusalem, Israel, August 1997

Determination of the Gluon Density in the Proton from Deep Inelastic ep Charm Production using NLO QCD

H1 Collaboration

Abstract

With the H1 detector at the ep collider HERA, D^* meson production cross sections have been measured in deep inelastic scattering with 4-momentum transfers $Q^2 > 2$ GeV$^2/c^2$. Using a Next-to-Leading Order QCD calculation, the gluon momentum distribution in the proton, $x_g g(x_g)$, has been extracted in the momentum fraction range $7.5 \cdot 10^{-4} < x_g < 2.5 \cdot 10^{-2}$, at an average scale $\mu^2 = 24$ GeV$^2/c^2$. The gluon momentum fraction x_g has been approximately reconstructed from the measured kinematics of the scattered electron and the D^* meson in the final state.

Abstract 275
Parallel Sessions 2,3,4,5
Plenary Sessions 1,2,3,6

1 Introduction

The most precise determinations of the gluon momentum distribution in the proton have been obtained from the analysis of scaling violations of the deep inelastic proton structure function F_2 [1, 2]. This method is however indirect in the sense that F_2 at low values of the Bjorken scaling variable x_B actually probes the sea quark distributions which are related via the QCD evolution equations to the gluon distribution. The local behavior of F_2 depends on the gluon distribution $g(x_g)$ in a rather wide range of momentum fractions x_g, and the analysis requires the assumption of a certain functional form of $g(x)$, the parameters of which are then determined in a fit procedure.

The production of heavy quarks in electron proton interactions proceeds, in QCD, almost exclusively via photon gluon fusion, where a photon coupling to the incoming electron interacts with a gluon in the proton by forming a quark-anti-quark pair. The charm contribution to the proton structure function, $F_2^{c\bar{c}}$, was found to be well reproduced by such a description in Next to Leading Order (NLO) QCD [3].

More direct determinations of the gluon density can be obtained by partial reconstruction of the kinematics of the interacting partons from the measurement of the hadronic final state in gluon-induced processes. Such direct measurements are complementary to the indirect analyses: although limited in statistics, they are in principle more sensitive to local variations of the gluon distribution. They are affected by different systematics and provide an independent check of the underlying concepts. Direct gluon density determinations have previously been performed using dijet events [4, 5]. Compared to the jet case, smaller invariant masses of the partonic sub-process can be accessed in charm production. It is thus possible to extend the measurement towards smaller momentum fractions x_g. Also there is much less background from quark-induced processes.

Recently, Next-to-Leading-Order (NLO) QCD calculations of fully differential charm cross sections in DIS at HERA have become available [6, 7]. In the analysis presented here, these calculations are used to directly determine $g(x_g)$ in NLO from the measurement of D^* production cross sections with the H1 detector. The theoretical framework and the principle of the analysis will be described in more detail in the next section. In Section 3 the cross section measurement will be presented, and Section 4 will explain the method to extract the gluon density. The note concludes with a comparison with results obtained by H1 from the analysis of F_2.

2 Principle

Differential charm production cross sections in DIS have been calculated [8] in NLO QCD in the $\overline{\text{MS}}$ renormalization scheme. The computation was carried out using the subtraction method, which is based on the replacement of divergent soft and collinear terms in the squared matrix elements by generalized distributions. Charm quarks are treated as massive particles appearing only in the final state whereas the three light flavors (and gluons) are the only active partons in the initial state ("Three Flavour Number Scheme"). In leading order, production proceeds via the partonic sub-process $\gamma^* g \to c\bar{c}$. In NLO, there are in addition diagrams where a gluon is radiated from a gluon or a quark line, $\gamma^* g \to c\bar{c}g$, and quark induced processes $\gamma^* q \to c\bar{c}q$ and $\gamma^* \bar{q} \to c\bar{c}\bar{q}$.

Since the calculation is fully differential, it has access to the 4-vectors of all outgoing partons. The integration of cross sections can thus be performed using a Monte Carlo type program HVQDIS [7]. Moreover, this also allows to model the effect of charm quark fragmentation into D^* mesons. This is performed in the program by convolution of the charm quark cross section with a Peterson-Zerwas fragmentation function [9]; the D^* 3-momentum vector is formed by scaling the quark 3-momentum vector, and the D^* energy is fixed such that the mass is $m(D^*) = 2.01$ GeV/c^2. Evolution of the fragmentation function, which one expects to become important for transverse momenta $p_\perp \gg m_c$, is not included because the region of interest is $p_\perp \sim m_c$ ($m_c =$ charm quark mass). In this framework, visible cross sections (incorporating experimental cuts) can be calculated in NLO as a function of any final state variable depending on the D^* and electron 4-momenta. The cross sections can then be confronted to experimental data at hadron level.

The kinematics of the leading order $2 \to 2$ process $\gamma^* g \to c\bar{c}$ is fully determined if one incoming and one outgoing particle, here the photon and the charm (anti-)quark, are measured. The momentum fraction x_g is given by

$$x_g = x_B \left(1 + \frac{M^2}{Q^2}\right) \quad \text{with} \quad M^2 = \frac{p_{\perp c}^{*2} + m_c^2}{z(1-z)} \quad \text{and} \quad z \equiv \frac{p \cdot c}{p \cdot q} = \frac{(E - p_z)_c^{(\mathrm{Lab})}}{2yE_{\mathrm{beam}}} \tag{1}$$

where $p_{\perp c}^*$ is the transverse momentum of the charm quark in the photon proton center of mass frame, with respect to the axis defined by the incoming proton momentum in this frame. z is a Lorentz invariant that can be evaluated in the laboratory frame from the charm quark's energy E and momentum component p_z along the axis defined by the incident proton beam. $Q^2 = -q^2$ is the negative 4-momentum transfer from the scattered electron and $x_B = Q^2/(2p \cdot q)$ the Bjorken scaling variable; p is the incoming proton and c the outgoing (anti-)charm 4-momentum. $y = Q^2/x_B s$, $\sqrt{s}$ is the ep center of mass energy, and E_{beam} the electron beam energy in HERA.

In the presence of gluon radiation, the above relation holds only approximately. Also, in the experiment one measures not quarks but D^* mesons that carry only a fraction of the c quark's energy. However, with the replacements

$$p_{\perp c}^* \to 1.2\, p_{\perp D^*}^* \,, \quad (E - p_z)_c \to (E - p_z)_{D^*} \,, \quad x_g \to x_g^{OBS} \tag{2}$$

one can construct a hadronic observable x_g^{OBS} that is well correlated with x_g.

The calculation of the visible cross section $\sigma(x_g^{OBS})$ can be written as

$$\sigma(x_g^{OBS}) = \int_{x_{g,min}}^1 dx_g \, \left[g(x_g, \mu^2) \cdot \hat{\sigma}(x_g^{OBS}, x_g, \mu^2)\right] + \sigma_{quark}(x_g^{OBS}) \tag{3}$$

where μ is the factorization scale and $\hat{\sigma}$ plays the role of a partonic cross section, which is integrated over the remaining kinematic degrees of freedom and also depends on the experimental acceptance. It receives the dominant contributions from regions where $x_g \approx x_g^{OBS}$. σ_{quark} denotes the quark-induced contribution to the visible cross section. The form of Equation 3 is such that a determination of the gluon density in the proton can be made from the measured cross section by means of an unfolding procedure.

The analysis proceeds in two main steps. First, the visible D^* cross section is measured as a function of x_g^{OBS}. The data are corrected only for detector effects to the hadron level. Since there is no extrapolation into unmeasured regions nor any parton hadron correlation involved, this step can be performed using the leading order Monte Carlo program AROMA [10] which describes the final state well.

In the second step the cross section is unfolded to the true variable x_g and the gluon density $g(x_g, \mu^2)$ is extracted. This step is carried out in the framework of the Three Flavour Number Scheme. The NLO program HVQDIS is used to calculate the cross sections as a function of x_g^{OBS} as well as the correlations used for the unfolding, taking into account gluon radiation and fragmentation effects that both influence the correlation between hadronic and partonic quantities.

3 Cross Section Measurement

The cross section for the process $ep \to eD^*X$ has been measured in the visible range $2 < Q^2 < 100$ GeV^2/c^2, $0.01 < y < 0.7$, $p_\perp(D^*) > 1.5$ GeV/c and $|\eta(D^*)| < 1.5$, where $\eta = -\ln\tan(\theta/2)$ is the pseudo-rapidity and $p_\perp$ and θ are defined in the laboratory frame, with the z axis along the incident p beam direction.

The H1 detector and its trigger capabilities have been described elsewhere [11]. The data used here have been taken during 1995 when HERA was running with 27.5 GeV positrons (henceforth generically termed "electrons") colliding with 820 GeV protons. They correspond to a total integrated luminosity of $\mathcal{L} = 2.33$ pb^{-1}. The events have been triggered by an electromagnetic cluster in the rear lead scintillator "Spaghetti" calorimeter (SpaCal) [12] of at least 6.5 GeV energy, mostly in coincidence with a charged track signal from the multi-wire proportional chamber (MWPC) trigger and from the central drift chamber trigger.

The identification of electrons is similar to the procedure used in the inclusive structure function measurement [13]. The reconstruction of D^* mesons follows closely that in the previously published measurement of D^* photo-production [14].

Electrons are identified as clusters in the SpaCal with energy $E_e > 8$ GeV, with a cluster radius <3.5 cm consistent with electro-magnetic energy deposition, and with a cluster center matching within 2.5 cm to a charged track signal in the backward drift chamber [15]. The scattering angle was required to be $\theta_e < 177^o$.

The distribution of the electron energy for events containing a D^* candidate (as defined below) is shown in Fig 1a and compared to the AROMA Monte Carlo prediction which has been normalized to the data. The agreement is good in the region of the kinematic peak, which is sensitive to the energy calibration of the SpaCal, as well as in the region of smaller electron energies which is sensitive to possible background from photoproduction.

The Deep Inelastic Scattering kinematic variables are reconstructed using the "$e\Sigma$ method" [16]

$$Q^2 = 4E_{\text{beam}}E_e\cos^2\frac{\theta_e}{2} \quad \text{and} \quad y = \frac{2E_{\text{beam}}\sum_{had}(E-p_z)}{[\sum_{all}(E-p_z)]^2} \tag{4}$$

where the sum in the denominator runs over all (liquid Argon and SpaCal) calorimetric signals as well as central drift chamber tracks, avoiding double counting. The sum in the numerator is over all calorimeter signals except those forming the scattered electron candidate. This method is relatively robust against uncertainties in the electron energy scale and has small radiative corrections. y can also be measured using the electron alone, $y_e = 1 - (E_e/E_{\text{beam}})\sin^2(\theta_e/2)$, or using the hadronic final state alone, $y_\Sigma = (\sum_{had}(E-p_z)/2E_{\text{beam}}$. The ratio y_Σ/y_e is well described by the Monte Carlo simulation, as demonstrated in Fig 1b.

D^* mesons are reconstructed in the decay chain $D^{*+} \to D^0\pi^+_{slow} \to (K^-\pi^+)\pi^+_{slow}$ (the charge conjugate is always implied) for which the overall branching ratio is $BR(D^* \to K\pi\pi)$= 2.62% [17]. Tracks passing the quality cuts of Ref. [14] and fulfilling $p_\perp > 250(120)$ MeV/c were considered as K and π (π^+_{slow}) candidate. The invariant mass of the $K\pi$ combination had to be consistent with the D^0 mass within ± 80 MeV/c^2. In order to suppress combinatorial background, the range of z (Eqs. 1,2) has been restricted to $z > 0.2$.

The number of events, N_{D^*}, is extracted from fits to the distributions of the mass difference $\Delta M = M(K^-\pi^+\pi^+_{slow}) - M(K^-\pi^+)$ with a function taken to be a superposition of a Gaussian for the signal and a term $N_B(m-m_\pi)^a$ for the background. The position and width of the Gaussian are fixed to the values found from a higher statistics sample including photo-production events. The position is consistent with the table value [17], and the width agrees with simulation results.

The normalization of the signal, the background normalization N_B and shape exponent a are free parameters in the fit. The ΔM distribution for all D^* candidates in the whole visible region is shown together with the fit in Fig 2. A total of $N_{D^*} = 153 \pm 17$ events is observed. From Monte Carlo simulations the contribution to the signal due to D^0 decays into channels other than $K^-\pi^+$, is obtained to be $r = (7 \pm 4)\%$, for which a correction is made.

The cross section as function of x_g^{OBS} is measured by dividing the data sample into 4 bins of $\log_{10} x_g^{OBS}$ and determining the number of D^* mesons in each bin using this fit procedure. The effect of limited detector resolution on the variable x_g^{OBS} is small with respect to the bin size.

The electron and D^* reconstruction efficiencies are determined from simulations with the AROMA Monte Carlo program [10], using the MRS(G) parton density set [18], a charm quark mass of 1.5 GeV/c^2 and the renormalization scale μ given by the invariant mass of the γg system. The dependence of the simulated efficiencies on these choices was estimated to be small and was neglected. In Fig 3 it is shown that the observed rapidity and transverse momentum distributions of D^* mesons are acceptably reproduced. The efficiency is found to be ϵ_{reco} =40% on average, ranging from 28% in the lowest to 52% in the highest x_g^{OBS} bin. The trigger efficiency has been determined from data, by using independent trigger conditions, to be ϵ_{trig} =98.6%.

There is no indication of photoproduction background seen in the data; the electron energy and y_Σ distributions are consistent with expectations for a pure sample of DIS events. From simulations of direct and resolved charm photoproduction, using the AROMA and the PYTHIA [19] Monte Carlo generators, respectively, we expect less than 1 event within the cuts specified. No subtraction is therefore made and a 1% error attributed to this possible background source.

Background from $b\bar{b}$ production, with subsequent decays of b flavoured hadrons into D^* mesons, has been calculated using the AROMA generator to be about $N_B = 1.6$ events in total and subtracted from the number of events in each bin. The systematic error assigned to this contribution allows for a variation of the $b\bar{b}$ cross section within a factor of 3 of its predicted value.

Radiative corrections have been calculated using the analytic program HERACLES [20]. They amount to $\delta_{rad} = 3.3\%$ on average and depend only very weakly on y.

The cross section is obtained as

$$\sigma_{vis} = \frac{N_{D^*}(1-r) - N_B}{\epsilon_{trig}\epsilon_{rec}\, BR(D^* \to K\pi\pi)\, \mathcal{L}\, (1+\delta_{rad})} = (5.63 \pm 0.66^{+0.84}_{-0.68})\text{nb}\ , \qquad (5)$$

where the first error is statistical, the second is systematic and is detailed in Table 1. All contributions show only slight variation with x_g^{OBS}.

In Fig 4 the cross section results are shown as function of $p_\perp(D^*)$, $p_\perp^*(D^*)$, $\eta(D^*)$, Q^2, and x_B and compared to NLO QCD, using the GRV 94 HO parton distribution set [21] and a charm mass $m_c = 1.5$ GeV/c^2. The agreement is very good.

4 Extraction of the Gluon Density

The measured cross section $\sigma(x_g^{OBS})$ is compared to the NLO QCD prediction in Fig 5. The calculation was done with the HVQDIS program version 1.1 [7] using the GRV 94 HO parton density set [21]. The charm quark mass was set to $m_c = 1.5$ GeV/c^2, the QCD factorization and renormalization scales were set to $\mu = \sqrt{4m_c^2 + Q^2}$. For the $c \to D^*$ fragmentation fraction, the value 0.27 was used, consistent with the LEP value of $0.71 \pm 0.05\%$ for the fragmentation and decay chain $c \to D^{*+} \to K^-\pi^+\pi^+$ [22]. The fragmentation parameter $\epsilon_c = 0.060$ was used as determined [23] from data. This is one of the parameter settings used by the authors in Ref. [7]. The CTEQ4F3 parton density set [24] is also consistent with the Three Flavour Number Scheme and was shown in [7] to yield results very close to those obtained with GRV 94 HO (see also Fig 7a). It is preferred for the subsequent analysis since $\Lambda^{(5)} = 225$ MeV yields the world average for the strong coupling constant, $\alpha_s(M_Z) = 0.118 \pm 0.003$ [17]. The dependence of the results on these choices will be included in the systematic error.

First, according to Eq. 3 the quark-induced contribution as predicted in the QCD calculation is subtracted from the data bin by bin. It is at the percent level; the correlation with the gluon density via QCD evolution can be neglected here, but the uncertainty arising from it will be included in the error.

The quark-subtracted cross section is converted into a cross section distribution as function of true x_g using the iterative unfolding procedure for binned distributions of Ref. [25]. The correlation between x_g^{OBS} and x_g as obtained from the QCD calculation is shown as two-dimensional histogram in Fig. 6. This correlation is used for the first unfolding iteration; for each next iteration it is re-weighted using the result of the previous one. After 4 steps at most, convergence is reached, and the "smeared" distribution $\sigma(x_g^{OBS})$ agrees with the measurement, as shown in Fig. 7a. The unfolded distribution is shown in Fig. 7b together with the QCD prediction which was the input to the first unfolding iteration (dashed) and the reweighted prediction used for the last one (solid). The covariance matrix of the result and correlations between adjacent bins will be discussed below in terms of the final gluon density.

The gluon density is extracted at an average scale given by the average $\langle Q^2 \rangle = 15$ GeV$^2/c^2$, $\mu_0^2 = 4m_c^2 + \langle Q \rangle^2 = 24$ GeV$^2/c^2$. The unfolded cross section distribution factorizes:

$$\sigma(x_{g,i}) = g(x_{g,i}, \mu_i^2) \cdot \tilde{\sigma}(x_{g,i}) \tag{6}$$

Table 1: *Applied corrections and systematic errors of the cross section measurements.*

Applied Corrections			
Effect	Corr.	Syst. Error ↑	Syst. Error ↓
Trigger efficiency	1.4%	5%	1.4%
γP background	0%	0%	1%
b-production background	1-2%	MC Pred.	3 × MC Pred.
Reflections	7%	4%	4%
Radiative corrections	≈ 3.3%	Correction	Correction
Systematic Errors			
Effect	Uncertainty	Syst. Error ↑	Syst. Error ↓
Energy scale Elm SpaCal	2% at 27GeV 3% at 7GeV	≈ 4%	≈ 4%
Electron angle	0.5 mrad	< 1%	< 1%
BDC hit finding		2%	2%
Energy scale Had SpaCal	7%	< 1%	< 1%
Energy scale LAr	4%	≈ 1%	≈ 1%
Luminosity		1.5%	1.5%
Track reconstruction		9%	3%
$D^{\star}$-Fit	from Fit with free Peak-Width	≈ 7%	≈ 7%
Branching ratio		4%	4%
Total		15.0%	12.2%

where μ_i is the average scale in bin i. The measured gluon density is calculated as

$$g(x_{g,i}, \mu_0^2) = \frac{g(x_{g,i}, \mu_0^2)^{\text{theory}}}{\sigma(x_{g,i})^{\text{theory}}} \cdot \sigma(x_{g,i})^{\text{experiment}} \tag{7}$$

Whereas the $\tilde{\sigma}(x_{g,i})$ are strictly independent of $g(x_g)$, the ratio in Eq. 7 also contains the variation of $g(x_{g,i}, \mu^2)$ when varying the scale from μ_i to μ_0. Since the measurement does not differentiate in Q^2, this is taken from theory. The variation is however small: the scale changes from 17 GeV^2 in the first to 28 GeV^2 in the last bin, and $g(x, \mu^2)$ deviates from $g(x, \mu_0^2)$ by not more than 9%. The effect is included in Eq. 7, and the dependence on the input parton density Q^2 variation is accounted for in the systematic error.

Systematic uncertainties affecting the gluon density extraction are determined by re-calculating with HVQDIS for different parameter choices the correlations and cross sections and re-analyzing the data starting from the measured cross section. The QCD factorization and renormalization scale μ is varied between $2m_c$ and $2\sqrt{4m_c^2 + Q^2}$, the charm quark mass m_c between 1.3 and 1.7 GeV/c^2, and the fragmentation parameter ϵ_c between 0.020 (as recently argued [26] for NLO calculations in the "massive charm" scheme) and 0.078 (as obtained from a combination of ARGUS and CLEO results [17]). In order to assess the dependence on the gluon density in the input parameterization, the MRS(D0') set[1] (already ruled out by HERA data [1, 2]) was used as an extreme choice. The uncertainty in the strong coupling constant (world average) is taken into account by variation of the scale $\Lambda^{(5)}$ between 176 and 248 MeV [17]. The systematic errors on $xg(x_g)$ as function of x_g are displayed as shaded bands in Figs. 8.

The resulting gluon distribution, $xg(x_g)$, is shown in Fig 9. The covariance matrix is given in Table 2. The error bars in the figure represent the diagonal elements only. The correlation coefficients (defined as $\rho_{ij} = \text{cov}_{ij}/\sqrt{\text{cov}_{ii}\text{cov}_{jj}}$) are 25%, 29%, 48% for the first, second and third pair of neighboring bins, respectively.

Table 2: *Covariance matrix for $xg(x_g)$. The first 4 rows and columns correspond to the 4 bins shown in Fig 9; correlations with the adjacent bin at high x_g are also included.*

19.680				
1.901	3.047			
0.150	0.484	0.889		
0.198	0.102	0.262	0.337	
-0.191	0.118	0.200	0.195	0.122

The contributions to the systematic error due to variations in the parameters of the theoretical model are added in quadrature and displayed as dark shaded histogram along the abscissa in Fig 9. An overall normalization uncertainty is induced by the experimental systematic error of the D^* cross section of 14%, increased by the additional uncertainty from the $c \to D^*$ fragmentation fraction, and it has to be added (in quadrature) on top of that to give the total systematic error shown as the larger shaded histogram. The errors are dominated by the statistical uncertainty. The largest contributions to the systematic error arises from the uncertainty of the charm quark mass.

The extracted gluon density can be compared to others determined in NLO from other processes. For example the new result of the QCD analysis of the scaling violations of F_2 for $xg(x_g)$ as obtained by H1 [27] is overlaid as well in Fig 9. This result has been obtained from a fit,

[1] This set is not consistent with the Three Flavour Number Scheme and is used only for practical purposes here.

using the NLO QCD evolution equations, to a fully inclusive structure function measurement. It agrees – within errors – well with the gluon distribution resulting from this analysis, performed in the framework of the Three Flavour Number Scheme as implemented in the HVQDIS program. This represents a non-trivial confirmation of the applied QCD concepts and of the universality of the parton distributions.

5 Conclusion

Using NLO QCD, a determination of the gluon density $g(x)$ has been performed from D^* cross sections in deep inelastic ep scattering at an average scale $\mu^2 = 24$ GeV^2/c^2. The gluon momentum fraction x has been approximated to x_g^{OBS} using the kinematic information from the D^* meson in addition to the scattered electron, and the visible cross section has been measured as a function of x_g^{OBS}. $xg(x)$ has been extracted in the Three Flavour Number Scheme as implemented in the HVQDIS program, which uses the Peterson-Zerwas form of the fragmentation function to model the nonperturbative hadronization process. The errors are dominated by the statistical uncertainty.

The overall description of the differential cross sections by the NLO QCD calculations has been found to be very good. The extracted gluon density agrees well with that obtained from the QCD analysis of the inclusive measurement of the proton structure function F_2.

Acknowledgements

We are grateful to the HERA machine group whose outstanding efforts have made and continue to make this experiment possible. We thank the engineers and technicians for their work in constructing and now maintaining the H1 detector, our funding agencies for financial support, the DESY technical staff for continual assistance, and the DESY directorate for the hospitality which they extend to the non-DESY members of the collaboration. We wish to thank B. Harris and J. Smith for assistance in the QCD calculations and many fruitful discussions.

References

[1] S. Aid *et al.* (H1 Collaboration), Nucl. Phys. B470 (1996) 3.

[2] M. Derrick *et al* (ZEUS Collaboration), Z. Phys. C72 (1996) 399;
M. Botje, QCD Analysis of ZEUS 1994 F_2 data, in Proceedings "Workshop on Deep Inelastic Scattering and Related Phenomena (DIS 97)", Chicago, April 1997.

[3] C. Adloff *et al* (H1 Collaboration), Z. Phys. C72 (1996) 593;
J. Breitweg *et al* (ZEUS Collaboration), preprint DESY 97-089 (May 1997).

[4] S. Aid *et al* (H1 Collaboration) Nucl. Phys. B449 (1995) 3.

[5] K. Rosenbauer, A direct Determination of the Strong Coupling Constant and the Gluon Density in the Proton in next-to-leading-order from (2+1)-Jet Rates in the H1-Experiment, in Proceedings "Workshop on Deep Inelastic Scattering and Related Phenomena (DIS 96)", Roma, April 1996.

[6] B.W. Harris, hep-ph/9608379, talk A05057 presented at the 1996 annual meeting of the Division of Particles and Fields, American Physical Society, Minneapolis, MN, August 1996. To appear in proceedings thereof.

[7] B.W. Harris and J. Smith, preprint DESY 97-111, FSU-HEP-970527, May 1997.

[8] B.W. Harris and J. Smith, Nucl. Phys. B452 (1995) 109; Phys. Lett. B353 (1995) 535.

[9] C. Peterson, D. Schlatter, I. Schmitt, and P.M. Zerwas, Phys. Rev. D 27 (1983) 105.

[10] G. Ingelman, J. Rathsman and G.A. Schuler, Comput. Phys. Commun. 101 (1997) 135.

[11] I. Abt *et al* (H1 Collaboration) Nucl. Instr. Meth. A386 (1997) 310 and 348.

[12] R.D. Appuhn *et al* (H1 SpaCal group), DESY preprint 96-171, submitted to Nucl. Inst. and Meth.

[13] C. Adloff *et al* (H1 Collaboration), preprint DESY 97-042, March 1997, submitted to Nucl. Phys. B.

[14] S. Aid *et al* (H1 Collaboration), Nucl. Phys. B472 (1996) 32.

[15] H1 collaboration, Technical proposal for the upgrade of the backward region of the H1 detector, DESY internal report PRC-93/02.

[16] U. Bassler and G. Bernardi, Nucl. Instrum. Meth. A361 (1995) 197.

[17] R.M. Barnett *et al* (Particle Data Group), Phys. Rev. D54 (1996) 1.

[18] A.D. Martin, R.G. Roberts, and W.J. Stirling, Phys. Lett. B354 (1995) 155.

[19] T. Sjöstrand, CERN-TH-6488 (1992), Comp. Phys. Comm. 82 (1994) 74.

[20] A. Kwiatkowski, H. Spiesberger, and H.J. Mohring, Comput. Phys. Commun. 69 (1992) 155.

[21] M. Glück, E. Reya, and A. Vogt, Z. Phys. C67 (1995) 433.

[22] ALEPH, DELPHI, L3 and OPAL Collab., Nucl. Instrum. Meth. A378 (1996) 101.

[23] J. Chrin, Z. Phys. C 36 (1987) 163.

[24] H. Lai *et al*, Phys. Rev. D 55 (1997) 1280.

[25] G. D'Agostini, Nucl. Instrum. Meth. A362 (1995) 487.

[26] M. Cacciari and M. Greco, Phys. Rev. D55 (1997) 7134.

[27] V. Chekelian, Invited talk at Lepton Photon Symposium, Hamburg, July 1997.

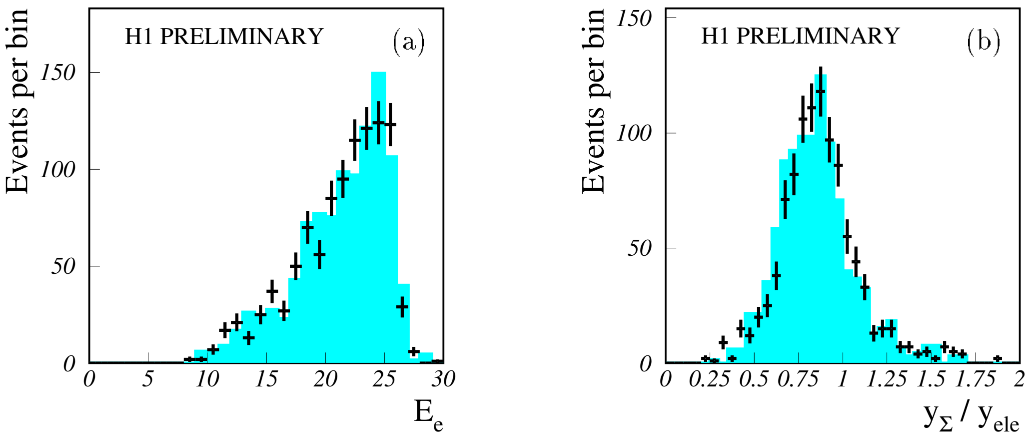

Figure 1: *a) Energy distribution for scattered electron candidates in the data (points with errors bars), for events containing a D^* candidate, compared with $ep \rightarrow D^*X$ Monte Carlo simulation (histogram), normalized to the data distribution. (b) Distribution of the ratio y_Σ/y_e for data (points) and Monte Carlo (histogram), normalized to data. (The "$e\Sigma$" method uses a combination of y_Σ and y_e.)*

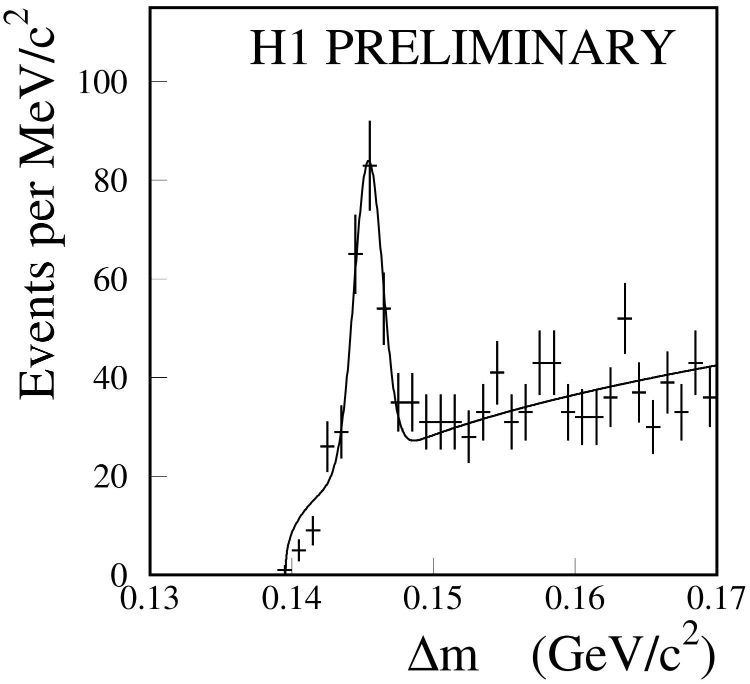

Figure 2: *Mass difference $\Delta M = M(K^-\pi^+\pi^+_{slow}) - M(K^-\pi^+)$ distribution of D^* candidates. The solid line represents the result of a fit as described in the text.*

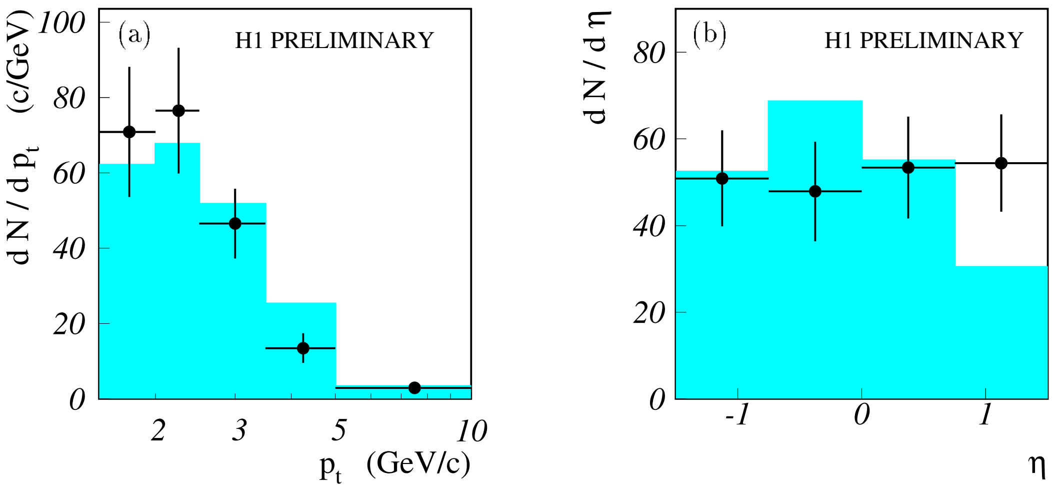

Figure 3: *a) Transverse momentum and b) pseudo-rapidity distribution of D^* candidates in data (points with errors bars) compared with $ep \to D^*X$ Monte Carlo simulation (histogram), normalized to the data distribution.*

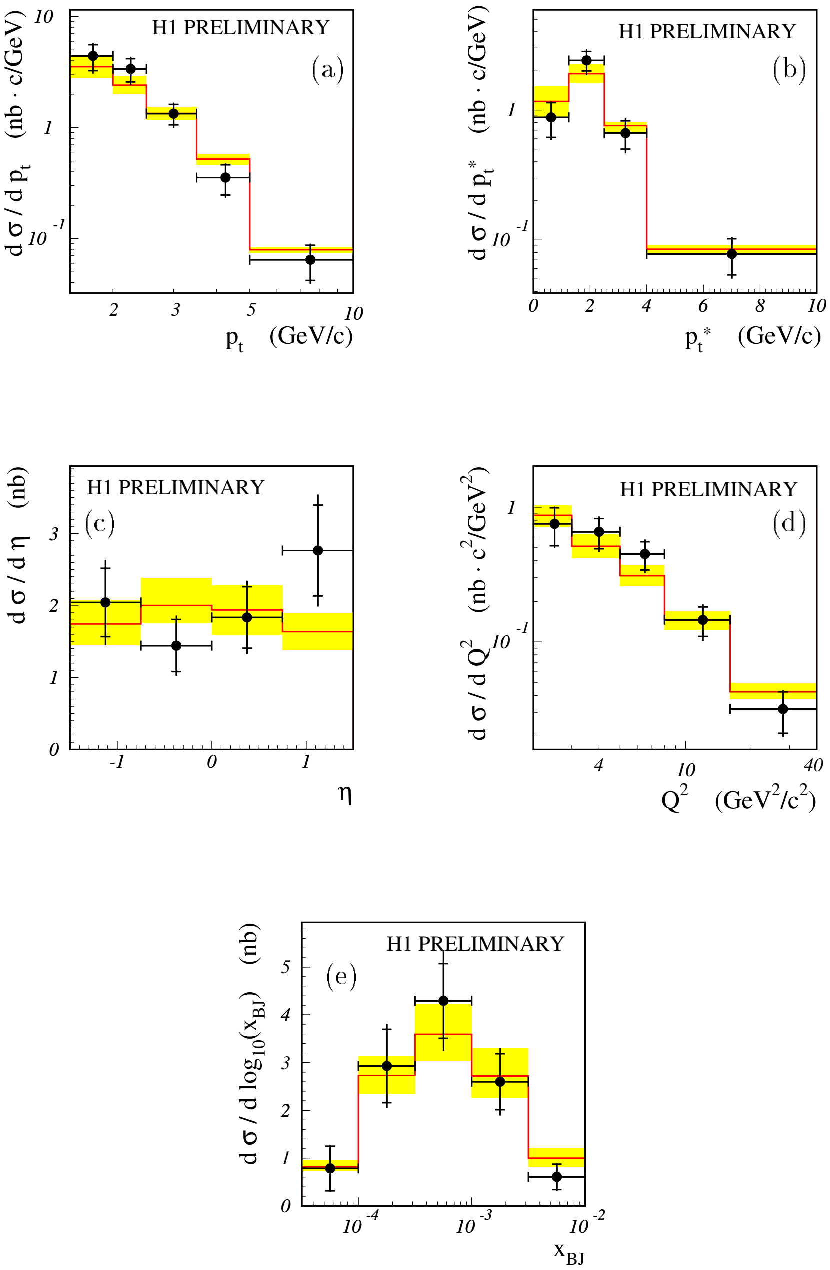

Figure 4: *Differential cross sections $\sigma(ep \to eD^*X)$ in the visible range (see text). The H1 data are shown as points with error bars, the NLO QCD prediction using the GRV 94 HO parton distribution set and a charm mass m_c = 1.5 GeV/c^2 is shown as a histogram. The shaded band represents the variation of the cross sections due to a variation of m_c between 1.3 and 1.7 GeV/c^2. (a) Transverse D^* momentum (in the lab frame), (b) Transverse D^* momentum (in the hadronic center of mass frame), (c) D^* pseudo-rapidity, (d) 4-momentum transfer Q^2, (e) x-Bjorken.*

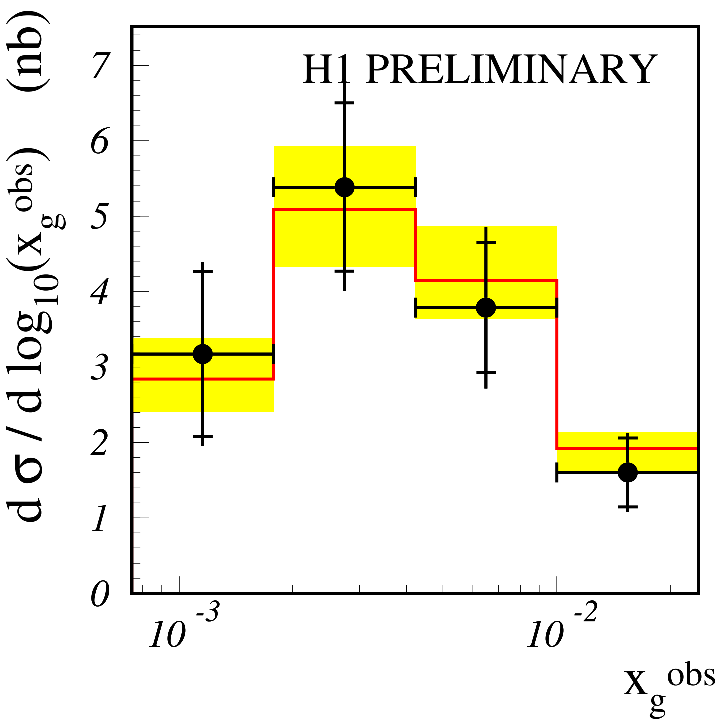

Figure 5: *Differential cross section $\sigma(ep \to eD^*X)$ as function of x_g^{OBS} in the visible range (see text). The H1 data are shown as points with error bars, the NLO QCD prediction using the GRV 94 HO parton distribution set is shown as a solid histogram. The shaded band represents the variation of the cross sections due to a variation of m_c between 1.3 and 1.7* GeV/c^2.

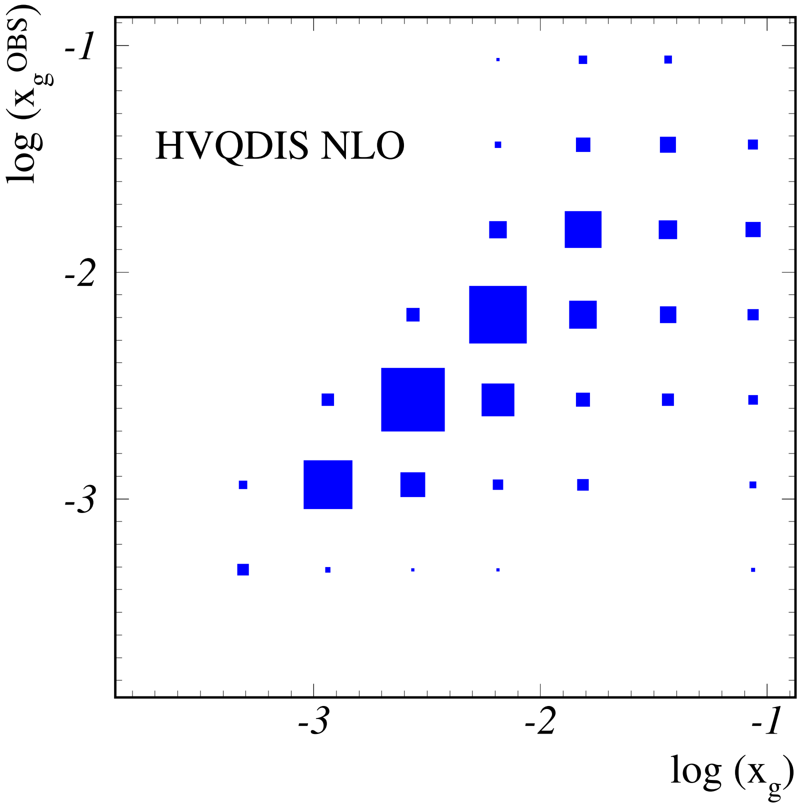

Figure 6: *Correlation between x_g^{OBS} as reconstructed from the D^* and electron momenta, and true momentum fraction x_g as predicted in NLO QCD, using the CTEQ4F3 parton distribution set. The bin area corresponds to the cross section contribution from the x_g interval to the measured x_g^{OBS} range.*

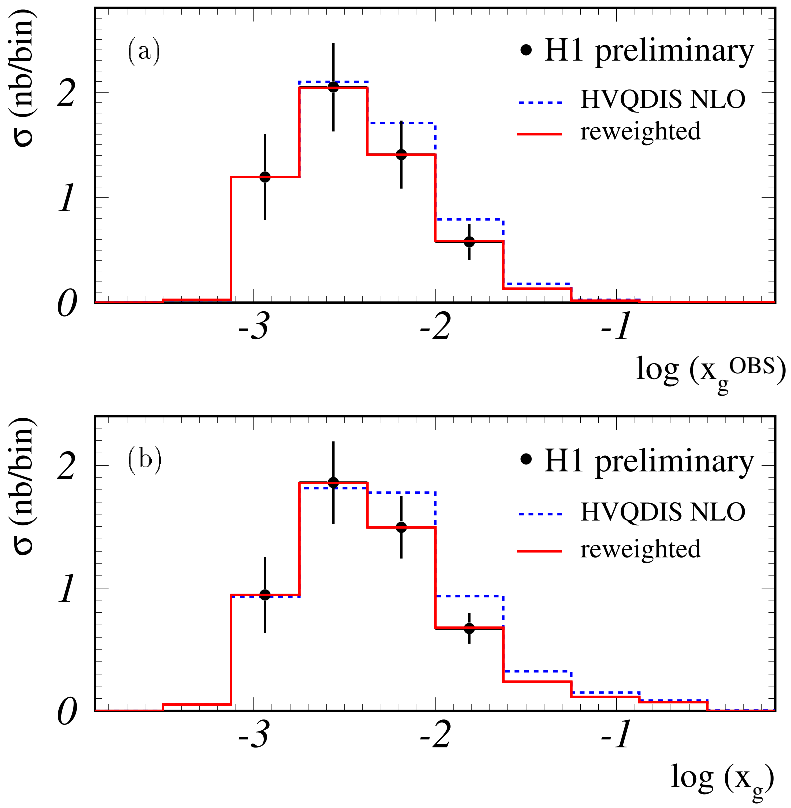

Figure 7: *a) Differential cross section $\sigma(ep \to eD^*X)$ (per bin) as function of x_g^{OBS} in the visible range (see text). The H1 data are shown as points with error bars, the NLO QCD prediction using the CTEQ4F3 parton distribution set is shown as a dashed histogram. The full histogram shows the prediction after re-weighting as function of true x_g with the result of the unfolding procedure. b) Unfolded cross section distribution versus true x_g. The dashed histogram is the NLO QCD prediction using CTEQ4F3, the solid histogram is the result of the last but one iteration as used for the calculation of re-weighted correlations.*

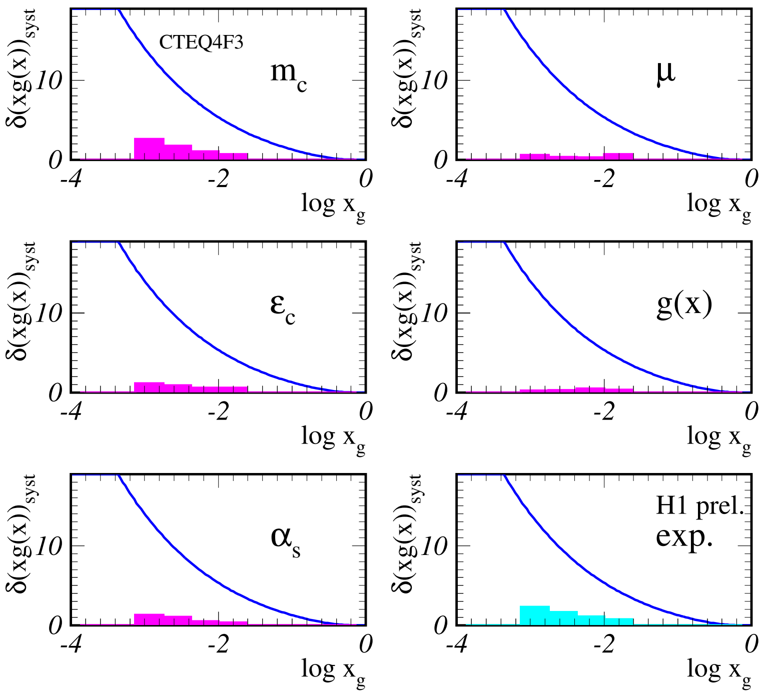

Figure 8: *Systematic uncertainty in $xg(x_g)$ as function of x_g, displayed as shaded band. For reference, the CTEQ4F3 parameterization for $\mu^2 = 24$ GeV$^2/c^2$ is also shown as solid line. Separately presented are the contributions due to variations of the QCD scale μ, the charm mass m_c, the fragmentation parameter ϵ_c, the strong coupling constant α_s, the parton density set used as input to the unfolding procedure, the experimental systematic uncertainty (including $BR(c \to D^*)$).*

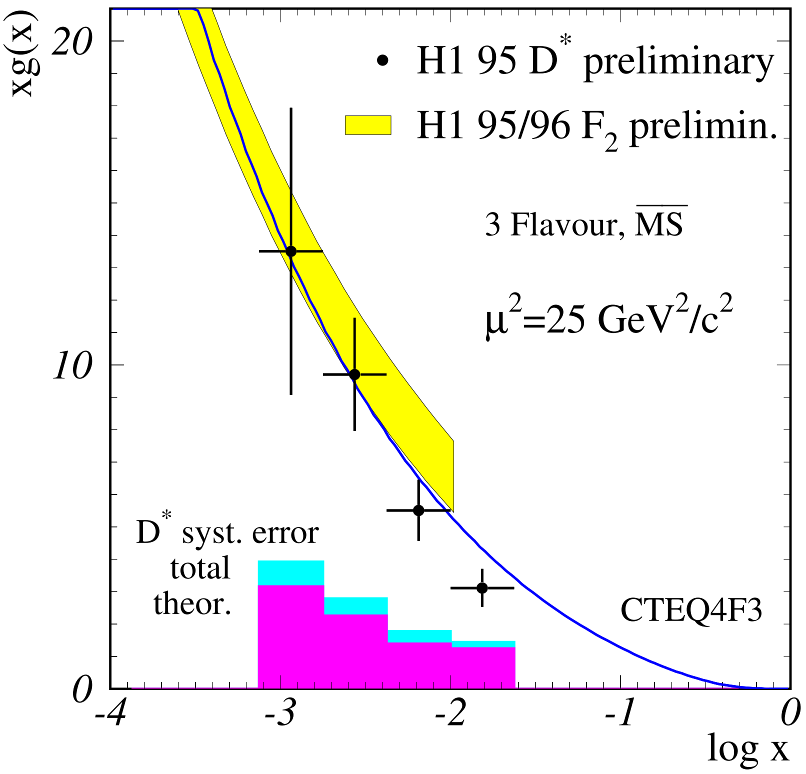

Figure 9: *Result (data points, with statistical errors only), theoretical and total systematic error (dark shaded and shaded bands along abscissa), compared to the CTEQ4F3 parameterization at $\mu^2 = 24$ GeV^2/c^2 (full line), and to the result of the H1 QCD analysis of the inclusive F_2 measurement at $\mu^2 = 25$ GeV^2/c^2 (light shaded band).*